Masked Faces with Faced Masks

Jiayi Zhu[1], Qing Guo[2], Felix Juefei-Xu[3], Yihao Huang[1], Yang Liu[2], Geguang Pu[1]

[1] East China Normal University, China
[2] Nanyang Technological University, Singapore
[3] Alibaba Group, USA

(a) Commercial Off-the-shelf Faced Mask

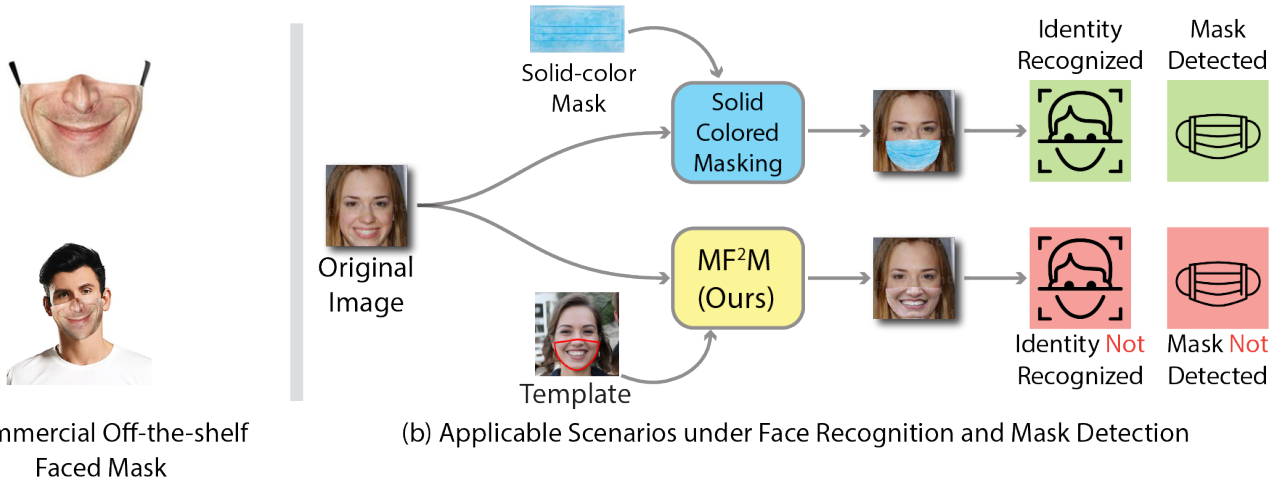(b) Applicable Scenarios under Face Recognition and Mask Detection

Figure 1: (a) shows a commercial off-the-shelf (COTS) faced mask and the look of being worn. (b) represents the security problem we are exploring. Faces wearing solid-color masks will be recognized as their original identities in most cases and easily detected by a mask detector (the upper arrow). The MF^{2}M we proposed extracts the face information in the area surrounded by the red line of the template image to obtain a "faced mask", which can simultaneously deceive face recognizers and evade mask detection (the lower arrow).

ABSTRACT

Modern face recognition systems (FRS) still fall short when the subjects are wearing facial masks, a common theme in the age of respiratory pandemics. An intuitive partial remedy is to add a mask detector to flag any masked faces so that the FRS can act accordingly for those low-confidence masked faces. In this work, we set out to investigate the potential vulnerability of such FRS equipped with a mask detector, on large-scale masked faces, which might trigger a serious risk, *e.g.*, letting a suspect evade the FRS where both facial identity and mask are undetected. As existing face recognizers and mask detectors have high performance in their respective tasks, *it is significantly challenging to simultaneously fool them and preserve the transferability of the attack*. We formulate the new task as the generation of realistic & adversarial-faced mask and make three main contributions: *First*, we study the naive *Delanunay-based masking method (DM)* to simulate the process of wearing a faced mask that is cropped from a template image, which reveals the main challenges of this new task. *Second*, we further equip the DM with the adversarial noise attack and propose the *adversarial noise Delaunay-based masking method (AdvNoise-DM)* that can fool the face recognition and mask detection effectively but make the face less natural. *Third*, we propose the *adversarial filtering Delaunay-based masking method* denoted as MF^{2}M by employing the adversarial filtering for AdvNoise-DM and obtain more natural faces. With the above efforts, the final version not only leads to significant performance deterioration of the state-of-the-art (SOTA) deep learning-based FRS, but also remains undetected by the SOTA facial

mask detector, thus successfully fooling both systems at the same time. We conduct extensive white-box and black-box experiments on three FRS and a facial mask detector. We utilize the datasets in MegaFace Challenge 1 and evaluate on dimensions of face recognition, face verification and mask detection, comparing with the solid-colored masking method and seven SOTA adversarial attacks. Moreover, we also set up the physical experiments by printing the adversarial faces in the real world and re-capturing them to fool the face recognition and mask detector, which demonstrates the high generalizability of our method. Overall, the proposed method, for the first attempt, unveils the vulnerability of the FRS when dealing with masked faces wearing faced masks.

KEYWORDS

face recognition, mask detection, adversarial attack, pixel-wise filtering

1 INTRODUCTION

Currently, under the severe international situation and environment (*i.e.*, COVID-19 pandemic), people are mandatorily required to wear facial masks in public, especially in crowded places like airports. This situation poses a huge challenge for face recognition systems (FRS). Although existing face recognition models (*e.g.*, SphereFace [27], CosFace [42], ArcFace [5]) have high-performance on identity recognition tasks, these models are only available to faces in good imagery conditions. When faces are heavily obscured (*e.g.*, wearing facial masks), even the state-of-the-art (SOTA) FRS do

not perform satisfactorily since the information of the masked area is lost. Recently, the National Institute of Standards and Technology (NIST) published a specific study to confirm that the accuracy of FRS drops sharply targeting masked faces [33].

An indirect way to solve this problem is to do mask detection. Once a facial mask is detected, the inspector can be made aware of the inaccuracy of the current face recognition result and respond accordingly. However, there are various styles of commercial off-the-shelf (COTS) facial masks, even some faced masks (*i.e.*, printed with the lower half of faces from celebrities) as shown in Fig. 1(a). Such COTS faced masks cause great confusion to existing mask detectors as these detectors only consider solid-colored masks (*e.g.*, common surgical masks) during training. Therefore, existing mask detectors can not deal with masks with special textures and complex patterns. It is worrying that potential offenders may wear such COTS faced masks and even do special treatment to viciously hide their identities and avoid mask detection at the same time. To explore this security problem, we simulate the process of manufacturing masks with face patterns and propose "faced mask" approaches. Our approaches attack both the FRS and the mask detector, exposing their weaknesses under this specific multitasking attack.

In this paper, we propose an adversarial filtering Delaunay-based masking method, denotes as **Masked Faces with Faced Masks** (MF^2M), to stealthily generate masks with face patterns. The perpetrating faced masks not only significantly reduce the accuracy of two SOTA deep learning-based FRS but also drop the accuracy of a SOTA mask detector by 83.58%. As shown in Fig. 1(b), faces wearing solid-colored masks will be recognized as their original identities in most cases and easily detected by a mask detector (the upper arrow). The MF^2M we proposed (the lower arrow) can simultaneously deceive face recognizers and evade mask detection. In particular, we first modify the Delaunay method [31] to simulate the process of wearing masks and propose a Delaunay-based masking method. We replace the lower face of the input image (*i.e.*, the original image in Fig. 1(b)) with the lower face of the desired face image (*i.e.*, the area surrounded by the red line of the template image in Fig. 1(b)). Intuitively, adding adversarial noise to the mask can successfully attack both the face recognition and mask detection systems. However, our experiments show that this method will cause the pixels to be strongly modified. To make up for this deficiency and make images look more natural, we further exploit the advantages of filters and propose the novel filtering-based attack method MF^2M.

Since the FRS mainly takes features of the eye area (also known as the periocular region [16–20]) into consideration, attacking the FRS through only modifying the lower face is much more difficult than modifying the upper face. To our best knowledge, previous methods all attack the FRS by modifying the upper face area [23, 36, 49]. Our method is the first attempt which only changes the lower face area to attack the FRS. Furthermore, our method (*i.e.*, MF^2M) can both be used as white-box and black-box attacks to the SOTA FRS, which reflects its usability and universality.

The contributions are summarized as follows. ❶ We study the naive Delanunay-based masking method (DM) to simulate the process of wearing a faced mask, which reveals the main challenge that this operation of only replacing the lower face does not strongly interference discriminators. ❷ We further equip the DM with the adversarial noise attack and propose the adversarial noise Delaunay-based masking method (AdvNoise-DM) that can handle the joint-task that fools the face recognition and mask detection effectively. ❸ We propose the adversarial filtering Delaunay-based masking method (denoted as MF^2M) by employing the adversarial filtering for AdvNoise-DM. This masking method leads to significant performance deterioration of SOTA deep learning-based face recognizers and mask detector while ensuring the naturalness of the obtained faces. ❹ Our extensive experiments in white-box attack and black-box attack demonstrate the universality and transferability of our proposed MF^2M. Then we extend to physical attack and illustrate the robustness of our proposed masking method.

2 RELATED WORK

Face recognition. Face recognition can be divided into closed-set recognition and open-set recognition. For closed-set recognition, the identities in the test set need to be included in the training datasets. This task is regarded as a multi-class classification problem and is usually solved by a softmax classifier [4, 34, 38, 39, 45]. Currently, most face recognition researches focus on open-set recognition (*i.e.*, identities for testing do not exist in the training datasets). A series of algorithms were proposed to learn an embedding to represent each identity [5, 27, 28, 41, 42, 47, 50]. Those algorithms modify the loss function to maximize inter-class variance and minimize intra-class variance. SphereFace [27] pioneered an angular softmax loss to learn angularly discriminative features. CosFace [42] presented a large margin cosine loss to remove radial variations. ArcFace [5] proposed an additive angular margin loss. Although these methods show high performance on the face recognition task under good imagery conditions, they pay little attention to obscured faces and are incompetent with masked faces recognition.

To tackle this problem, some researchers added specific modules to adjust existing models and strengthen the recognition performance for masked faces [2, 25, 32]. Recently, Masked Face Recognition Competition (MFR 2021) [3] was held to promote masked face recognition accuracy. Almost all of the participants utilized variations of the ArcFace as their loss and exploited either real or simulated solid-colored masked face images as part of their training datasets. These masked face recognition methods showed better robustness regarding faces masked with solid-colored masks. However, these methods do not solve the problem essentially, not considering masks with face patterns and special textures.

Mask detection. In the age of the outbreak of the COVID-19 pandemic, researchers pay more attention to masked face detection and relative datasets. The Masked Faces (MAFA) dataset [12] is an early proposed dataset for occluded face detection, which is collected from the Internet, varying in pose angle and occlusion degree. Recently, Wuhan University has introduced the Real-world Masked Face Recognition Dataset (RMFRD) and the Simulated Masked Face Recognition Dataset (SMFRD) [46]. These datasets all focus on masks with solid colors and ignore masks with specific textures or complex patterns. To judge whether there is a mask, some mask detection methods fine-tune face detection models to meet the requirement [1, 29, 35]. Although these methods perform well on common mask detection, they can not deal with special masks with facial textures as they ignore this situation.
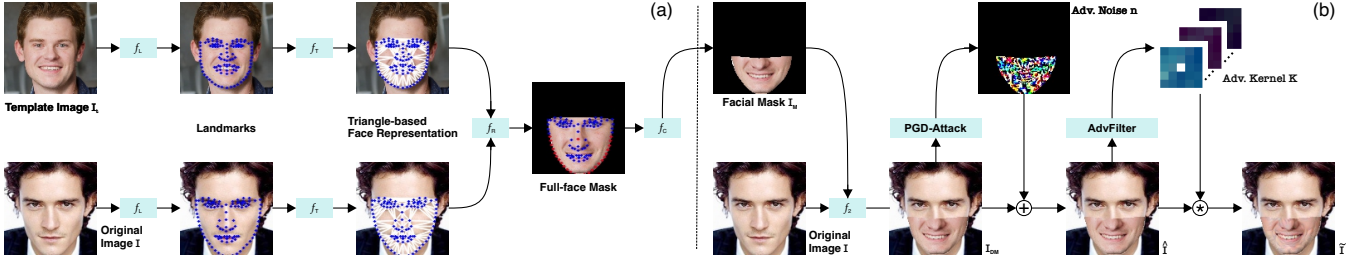
Figure 2: (a) shows process of generating the faced mask from the original image and the template image. (b) shows the pipeline of the proposed Delaunay-based Masking method, AdvNoise-DM, and MF^{2}M.
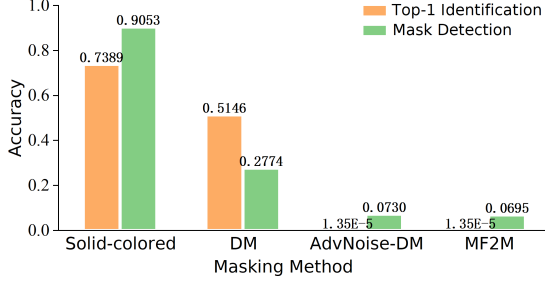

Figure 3: Top-1 identification rates and mask detection rates for solid-colored mask, DM, AdvNoise-DM and MF^{2}M on MegaFace Challenge 1.

Adversarial attack. There are a series of adversarial attacks. The fast gradient sign method (FGSM) [13] first proposes the additive-perturbation-based attack and the iterative fast gradient sign method (I-FGSM) [24] is an iterative variant of FGSM. Then the momentum iterative fast gradient sign method (MI-FGSM) [9] introduces the idea of momentum, which helps to stabilize optimization and escape from poor local maxima in the iteration. Besides, the translation-invariant fast gradient sign method (TI-FGSM) [10] and the diverse inputs iterative fast gradient sign method (DI^2-FGSM) [48] are both designed for transferability and apply transformations to the input images at each iteration in the attack process. TI-FGSM utilizes a kernel matrix to simulate the translation of images in different directions while DI^2-FGSM applies random resizing and padding to images with a given probability. More recently, a series of works focus on natural degradation-based adversarial attacks like adversarial morphing attack against face recognition [43], adversarial relighting attack [11], adversarial blur attack [14, 15], and adversarial vignetting attack [40]. These works explore the robustness of deep models by adding natural degradations like motion blur and light variation to the input with different adversarial objective functions. In this work, we actually regard the faced masks as the real-world perturbations.

3 METHODOLOGY

In order to illustrate the potential hazards of such faced masks, we propose a multi-stage framework to interfere with face recognizers and avoid mask detection simultaneously.

3.1 Delaunay-based Masking and Motivation

To simulate the process of wearing faced masks, the most intuitive way is to do an operation similar to face replacing in the specified area. We first apply a Delaunay-based masking method

(DM). This method operates on two images, one is an original image $I \in \mathbb{R}^{H_1 \times W_1 \times 3}$ on which we want to put the faced mask, the other is a template image $I_t \in \mathbb{R}^{H_2 \times W_2 \times 3}$ used to build the faced mask. The template image can be unreal and constructed by some DeepFake technique (*e.g.*, StyleGAN [21]). We aim to generate a facial mask that contains partial face patterns from I_t and looks natural when added to I with the process

$$I_M = f_1(I, I_t), \tag{1}$$

where $I_M \in \mathbb{R}^{H_1 \times W_1 \times 3}$ is the obtained mask (*e.g.*, facial mask in Fig. 2). Specifically, we expand the function $f_1(\cdot)$ as

$$f_1(I, I_t) = f_C(f_R(f_T(f_L(I_t)), f_T(f_L(I)))), \tag{2}$$

where $f_L(\cdot)$ extracts the landmarks of I_t and I as the first step of Fig. 2(a). The function $f_T(\cdot)$ is to build the triangle-based face representation where the landmarks serve as vertices of the triangles. The obtained face representations from I_t and I have the same number of triangles and those triangles correspond one by one according to the landmarks. As we have the correspondence of triangles between the two face representations, $f_R(\cdot)$ transforms each triangle in $f_T(f_L(I_t))$ into the corresponding triangle in $f_T(f_L(I))$ by affine transformation to get a full-face mask at the right side of Fig. 2(a). The function $f_C(\cdot)$ connects the landmarks of the contour of the lower face and the landmark of the nose (red dots in the full-face mask) in turn to obtain the faced mask area. As shown in the beginning of Fig. 2(b), after getting the facial mask I_M, we overlay it on the original image I to get the Delaunay-based masked image $I_{DM} \in \mathbb{R}^{H_1 \times W_1 \times 3}$ through

$$I_{DM} = f_2(I, I_M) = f_2(I, f_1(I, I_t)). \tag{3}$$

To better motivate our proposed method, we have carried out a pilot study. Here, we briefly discuss the results using images obtained by DM in face recognition and mask detection and compare them with the results of solid-color masked faces. We use the whole gallery set (1M images) and take 3,530 faces of 80 celebrities as the probe set from MegaFace Challenge 1 [22]. We compare the top-1 identification rates and the mask detection rates of images wearing solid-color medical masks and images generated by DM in Fig. 3. We can see that both indicators are very high when adding solid-colored medical masks, indicating that such masks hardly influence those discriminators. Images obtained by DM have a considerable impact to face recognizers and the mask detector. However, DM is not effective enough as shown in the second cluster of Fig. 3. There are still about 51% and 28% tasks judged correctly for top-1 identification and mask detection, respectively, far from zero. In order to strengthen the aggressiveness of the designed faced mask,

we propose adversarial masking methods to add special textures, as explained in the following sections.

The main challenges stem from: ❶ Most of the face information is concentrated in the eye region. In contrast, the part of the mask area, *e.g.*, the mouth, plays a relatively low role in the face recognition task, which increases the difficulty of our work. ❷ Although a part of images processed by DM can remain undetected by the facial mask detector, 28% of images are detected due to the unavoidable factors in the process of adding masks (*e.g.*, the chromatic aberration between faced masks and skins, discontinuities in textures), which makes interference to the mask detector unsuccessful. ❸ Our goal is to combine multiple tasks, and it is difficult to simultaneously handle tasks that have different optimization directions. ❹ Different deep-learning-based discriminators use different network structures and different network parameters. It is hard to ensure the transferability that the generated faced masks can effectively interfere with diverse discriminators.

3.2 Adversarial Noise Delaunay-based Masking

Inspired by adversarial attacks, *e.g.*, project gradient descent (PGD) [30], which performs effectively when targeting pre-trained neural networks, we apply an adversarial attack to the masked image $\mathbf{I_{DM}}$ acquired by DM. We define this method as an adversarial noise Delaunay-based masking method (AdvNoise-DM) and show the process in the middle of Fig. 2(b). We replace $\mathbf{I_{DM}}$ with Eq. (3) and generate the adversarial noise $\mathbf{n} \in \mathbb{R}^{H_1 \times W_1 \times 3}$ to obtain

$$\hat{\mathbf{I}} = f_2(\mathbf{I}, f_1(\mathbf{I}, \mathbf{I_t})) + \mathbf{n}, \tag{4}$$

which denotes the superimposition of the intermediate $f_2(\mathbf{I}, f_1(\mathbf{I}, \mathbf{I_t}))$ and the adversarial perturbation $\mathbf{n}$. Our goal is to find the $\hat{\mathbf{I}}$ which can not only mislead the FRS but also remain undetected by the mask detector by the means of obtaining such an adversarial perturbation $\mathbf{n}$. For this reason, the problem to be solved can be transformed into achieving the optimal trade-off between face recognition and mask detection. Then, we have the following objective function

$$\arg\max_{\mathbf{n}} \mathcal{D}(\text{FR}(f_2(\mathbf{I}, f_1(\mathbf{I}, \mathbf{I_t})) + \mathbf{n}), \text{FR}(\mathbf{I}))$$
$$- \alpha * \mathcal{J}(\text{MD}(f_2(\mathbf{I}, f_1(\mathbf{I}, \mathbf{I_t})) + \mathbf{n}), y). \tag{5}$$

In the first part of the objective function, $\text{FR}(\cdot)$ denotes a face recognition function which receives an image and returns the corresponding embedding. $\mathcal{D}(\cdot)$ denotes the Euclidean distance between the embedding from the original image $\mathbf{I}$ and the embedding from the image $\hat{\mathbf{I}}$ processed by AdvNoise-DM. We intend to maximize this part of the objective function for the purpose of enlarging the gap of identification information before and after the modification.

In the second part, $\text{MD}(\cdot)$ represents a mask detection function which receives an image and returns the probability of wearing a mask. $\mathcal{J}(\cdot)$ denotes the cross-entropy loss function, y is the ground truth label for whether the face is masked, 0 for not masked, and 1 for masked. Here, we set $y = 0$ to force the image $\hat{\mathbf{I}}$ to be judged without a mask. The ratio α is used to adjust the focus between face recognition and mask detection. We aim to minimize this cross-entropy loss so we take a minus sign for this item.

The images obtained by AdvNoise-DM can significantly interfere with the discrimination of face recognizers and the mask detector.
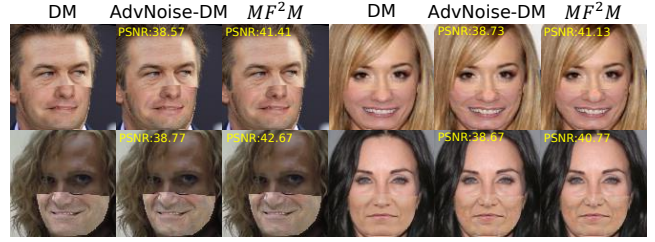

Figure 4: Examples to compare the PSNR values between AdvNoise-DM and MF²M. The PSNR value is calculated by the current image and the DM image.

This method can almost reduce the top-1 identification rate to zero and reduce the mask detection rate to only 7.3% as shown in Fig. 3. Nevertheless, AdvNoise-DM has a certain drawback as it causes great changes to the pixels, so reduces the naturalness of the generated images. In this case, it is necessary to use a smoother masking method.

3.3 Adversarial Filtering Delaunay-based Masking

Since the filtering process brings better smoothness, calculating each pixel by the surrounding pixels, we further propose an adversarial filtering Delaunay-based masking method (MF²M). This method combines noise-based and filtering-based attacks as shown in Fig. 2(b). We first apply DM and add a relatively small adversarial perturbation $\mathbf{n}$ to get the intermediate $f_2(\mathbf{I}, f_1(\mathbf{I}, \mathbf{I_t})) + \mathbf{n}$, referring to the method AdvNoise-DM. Then we utilize pixel-wise kernels $\mathbf{K} \in \mathbb{R}^{H_1 \times W_1 \times K^2}$ to process the intermediate. The p-th pixel of the intermediate $f_2(\mathbf{I}, f_1(\mathbf{I}, \mathbf{I_t})) + \mathbf{n}$ is processed by the corresponding p-th kernel in $\mathbf{K}$, denoted as $\mathbf{K}_p \in \mathbb{R}^{K \times K}$, where K represents the kernel size. We retouch the original image $\mathbf{I}$ via the guidance of filtering and reformulate Eq. (4) as

$$\tilde{\mathbf{I}} = \mathbf{K} \circledast (f_2(\mathbf{I}, f_1(\mathbf{I}, \mathbf{I_t})) + \mathbf{n}), \tag{6}$$

where $\circledast$ denotes the pixel-wise filtering process and $\tilde{\mathbf{I}} \in \mathbb{R}^{H_1 \times W_1 \times 3}$ represents the filtered images. In the MF²M procedure, we aim at obtaining a deceptive $\tilde{\mathbf{I}}$ in both face recognition task and mask detection task by altering the pixel-wise kernels $\mathbf{K}$. The objective function for optimization looks similar to Eq. (5) as following

$$\arg\max_{\mathbf{K}} \mathcal{D}(\text{FR}(\mathbf{K} \circledast (f_2(\mathbf{I}, f_1(\mathbf{I}, \mathbf{I_t})) + \mathbf{n})), \text{FR}(\mathbf{I}))$$
$$- \beta * \mathcal{J}(\text{MD}(\mathbf{K} \circledast (f_2(\mathbf{I}, f_1(\mathbf{I}, \mathbf{I_t})) + \mathbf{n})), y). \tag{7}$$

Compared with Eq. (5), the optimization objective becomes $\mathbf{K}$. We intend to increase the Euclidean distance between the embedding from the original image $\mathbf{I}$ and that from the filtered image $\tilde{\mathbf{I}}$. Meanwhile, we try to improve the probability that the filtered image $\tilde{\mathbf{I}}$ is judged not wearing a mask. The ratio of the mask detection part is marked as β. As shown in Fig. 3, almost all images generated by MF²M is deceptive for face recognition and only 6.95% images are detected wearing masks. Besides, MF²M brings higher naturalness than AdvNoise-DM. Fig. 4 shows that the peak signal-to-noise ratio (PSNR) calculated between MF²M and DM is higher than that calculated between AdvNoise-DM and DM, indicating that MF²M changes images less. We will use two similarity metrics in the experiment to prove this strong point.

Algorithm 1: MF^{2}M

Input: Original image **I**, Template image **I$_t$**, Ratio β, Face
recognizer FR($\cdot$), Mask detector MD($\cdot$), Step size ϵ,
Label y of not masked image, Iteration period **T**.
Output: Reconstruction image $\tilde{\mathbf{I}}$.

1 Generate **I$_{DM}$** by extracting the faced mask from **I$_t$** and
overlay it on **I** by Delaunay triangulation.

2 $\hat{\mathbf{I}} = \text{PGD}_{attack}(\mathbf{I_{DM}})$.

3 Initial filtering kernels **K**;

4 **for** i = 1 to **T** do

5   Generate filtered image **I$^{'}$** via **I$^{'}$** = **K** $\circledast$ $\hat{\mathbf{I}}$;

6   Calculate **Loss$_D$** via Euclidean distance function $\mathcal{D}$
     Loss$_D$ = $\mathcal{D}(\text{FR}(\mathbf{I}^{'}), \text{FR}(\mathbf{I}))$;

7   Calculate **Loss$_{CE}$** via cross-entropy loss function $\mathcal{J}$
     Loss$_{CE}$ = $\mathcal{J}(\text{MD}(\mathbf{I}^{'}), y)$;

8   Calculate the sum loss function **Loss** via
     Loss = **Loss$_D$** $- \beta *$ **Loss$_{CE}$**;

9   Update filtering kernels **K** via **K** = **K** $+ \epsilon * \nabla_{\mathbf{K}}$ **Loss**;

10 Apply image filtering to obtain reconstruction image $\tilde{\mathbf{I}}$ via
$\tilde{\mathbf{I}}$ = **K** $\circledast$ $\hat{\mathbf{I}}$;

3.4 Algorithm for MF^{2}M

Algorithm 1 summarizes our method. First, we apply DM to
complete the face replacing process, *i.e.*, generating a faced mask
extracted from **I$_t$** and overlaying it on **I** to obtain **I$_{DM}$**. Second, we
add an adversarial noise **n** to **I$_{DM}$** and obtain $\hat{\mathbf{I}}$. In the filtering attack
process, we initialize the filtering kernels **K** whose initial action is
to make the filtered image consistent with the original image (*i.e.*,
the weight of the center position of each kernel is 1, and the weight
of other positions is 0). In each iteration, we perform pixel-wise
filtering by current kernels **K** and **I$_{DM}$** to acquire the current filtered
image **I$^{'}$**. Then we calculate **Loss$_D$** and **Loss$_{CE}$**, via the Euclidean
distance function and the cross-entropy loss function, respectively.
These two loss functions constitute the final optimization objective
function by the ratio β. At the end of each iteration, we update
the filtering kernels **K** according to the product of the step size ϵ
and the gradient of the optimization objective. Finally, we use the
optimized kernels to embellish the aimed image $\tilde{\mathbf{I}}$.

4 EXPERIMENTS

4.1 Experimental Setup

Face recognition methods. In our white-box attack experiment,
the backbone of the face recognizer [6] is pre-trained ResNet50 un-
der ArcFace. The face recognizer takes cropped images (112×112)
as input and returns the final 512-D embedding features. To illus-
trate the transferability, we further use recognizers [8] pre-trained
under CosFace with ResNet34 and ResNet50 as the backbone respec-
tively to verify the black-box attack performance. We choose these
two FRS as ArcFace and CosFace perform SOTA in face recognition.

Mask detection methods. The mask detection method bases on
RetinaNet [26], an efficient one-stage objects detecting method.
The pre-trained model [37] we used is competitive in existing mask
detectors, achieving 91.3% mAP at the face_mask validation dataset

(including 1839 images). The mask detector outputs two probabili-
ties of not-masked and masked faces respectively. By comparing
these two probabilities, we can judge whether there is a mask.

Datasets. We utilize 1M images of 690K individuals in MegaFace
Challenge 1 as the gallery set. In terms of the probe set, we refer
to the setting of MegaFace [22] and use a subset of FaceScrub (*i.e.*,
3,530 images of 80 celebrities) for efficiency. For the template images
used to extract faced masks, we use StyleGAN to generate images
with seeds numbered from 1 to 13,000. As some generated images
have illumination or occlusion problems, we manually select 3,136
high-quality face images.

Evaluation settings. The face recognition evaluation is based on
masked/not-masked pairs. We add masks to images of the probe set
and remain images in the gallery not-masked. When adding masks,
we select the most similar face image to the original face image
from 3,136 template images according to the features extracted by
the face recognition model, which aims to make the masked faces
look more natural. In AdvNoise-DM, we use PGD attack to add
deliberate noise. The epsilon (maximum distortion of adversarial
example) is 0.04. The step size for each attack iteration is 0.001 while
the number of iterations is 40. The ratio α is set to 1. In MF^{2}M, we
add noise with an epsilon of 0.01. The kernel size of the pixel-wise
kernels is 5. When alter the pixel-wise kernels, the step size is 0.1
and the number of iterations is 160. Here we set the coefficient β to
1, same as α. All optimization objectives are restricted to the faced
mask area obtained by a deep learning-based method [7].

Baseline methods. We apply seven SOTA adversarial attack meth-
ods to the solid-colored medical masks as our baselines, including
FGSM, I-FGSM, MI-FGSM, TI-FGSM, TI-MI-FGSM, DI^2-FGSM, and
M-DI^2-FGSM. The epsilon of these baselines is 0.04, to maintain
the same attack intensity as AdvNoise-DM. The iterations number
involved in baselines is 40, and the momentum coefficient involved
is 1. The added perturbation is restricted to the facial mask area.

Metrics. For face recognition, we use the top-1 identification rate
in the face identification task, the true accept rate (TAR) at 10^{-6}
false accept rate (FAR) and the area under curve (AUC) in the face
verification task. For mask detection, we use the detection rate.
To reflect the degree of reconstructed modification and evaluate
the naturalness of the generated images, we further use the PSNR
and the structural similarity (SSIM) [44] to measure the similarity
between the adversarial masked results and the corresponding
images from DM. The region of the calculation for similarity metrics
is the whole image.

4.2 Comparison on White-box Attack

Face recognition has two main tasks, face identification and face
verification. Given a probe image and a gallery, identification aims
to find an image which has the same identity as the probe image
from the gallery, *i.e.*, 1 vs. N search task. The verification task sets
a threshold to judge whether two images have the same identity,
i.e., 1 vs. 1 comparison task.

Face identification. We constitute 151K pairs with the same iden-
tity from 3,530 face images of 80 celebrities. For each pair, we
take one image as the probe image and put the other image into
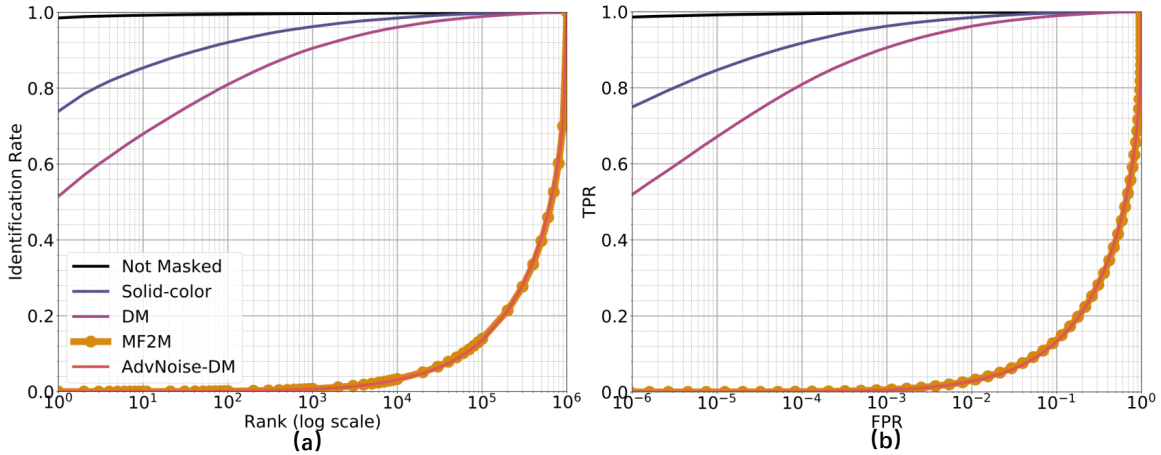
Figure 5: The effects of different masking methods on face recognition in white-box attacks. (a) The CMC curves of the face identification task. The abscissa indicates the number of images selected from the gallery. The ordinate denotes the identification rate at the specified number of images. (b) The ROC curves of the face verification task. The abscissa indicates the FPR and the ordinate denotes the TPR.

Table 1: Multifaceted evaluation of each masking method on white-box attack. "Rank 1" refers to the top-1 identification rate and "Veri." refers to the TAR at 10^{-6} FAR.

	Face Rec.	Face Verification		Mask Detection
	Rank 1	Veri.	AUC	Mask Rate
Solid-color	0.7389	0.7470	0.9986	90.53%
FGSM	0.4895	0.4924	0.9950	62.10%
I-FGSM	0.0039	0.0026	0.7594	39.41%
MI-FGSM	0.0179	0.0135	0.8667	43.91%
TI-FGSM	0.4991	0.5053	0.9950	66.00%
TI-MI-FGSM	0.0364	0.0290	0.8998	51.97%
DI^2-FGSM	0.0690	0.0601	0.9193	43.51%
M-DI^2-FGSM	0.0705	0.0623	0.9293	45.50%
DM (ours)	0.5146	0.5154	0.9956	27.74%
AdvNoise-DM (ours)	**1.35e^{-5}**	**1.35e^{-5}**	0.4163	7.30%
MF^{2}M (ours)	**1.35e^{-5}**	2.02e^{-5}	**0.4093**	**6.95%**

the gallery. Top-k identification rate denotes the successful rate of matching pairs where k is the number of images selected from the gallery. Fig. 5(a) shows the cumulative matching characteristic (CMC) curves of images under different masking states. The abscissa indicates the number of images selected from the gallery according to the embedding obtained by the face recognizer. The ordinate denotes the identification rate at the specified number of images. When images are without masks, the top-1 identification rate (*i.e.*, "Rank 1") is 0.98, proving that the recognizer achieves good performance without face occlusion. After adding solid-color medical masks, "Rank 1" reduces to 0.7389. This metric for DM declines to 0.5146. As for AdvNoise-DM and MF^{2}M, the higher the attack intensity, the more their corresponding curves are close to the lower right of the graph. We respectively alter the iterations numbers and make the performance of AdvNoise-DM and MF^{2}M close in this task, so as to compare them on other indicators. "Rank 1" of both methods drop to **1.35e^{-5}**, indicating that the SOTA face recognizer performs poorly under AdvNoise-DM and MF^{2}M. The second column of Table 1 shows that AdvNoise-DM and MF^{2}M achieve significantly lower "Rank 1" than seven SOTA additive-perturbation-based baselines.

Face verification. We use the 3,530 images of 80 identities in the probe set and 1M images in the gallery to build 151K positive samples and 3.5 billion negative samples for face verification. Fig. 5(b) shows the receiver operating characteristic (ROC) curves. We define the true positive rate (TPR) when the false positive rate (FPR) is $1e^{-6}$ as "Veri.", which is 0.7470 and 0.5154 for solid-color medical masks and DM, respectively. When we apply AdvNoise-DM and MF^{2}M, "Veri." almost drops to zero. In the third column and the fourth column of Table 1, we show the "Veri." values and the AUC values, respectively. We can see that both metrics of AdvNoise-DM and MF^{2}M are much lower than baselines.

Mask detection. We exhibit the mask detection rate of different masking methods in the fifth column of Table 1, which also represents the accuracy of the used mask detector. Solid-colored masks are easily detected and the detection rate is 90.53%. DM reduces the detection rate to 27.74%. AdvNoise-DM further interferes with the judgment of the detector and the accuracy decreases to only 7.30%. MF^{2}M achieves the best attack performance and reduces this rate to 6.95%. The detection rates for additive-perturbation-based baselines are between 39% and 66%. So far, we prove that our adversarial methods are very effective for both face recognition and mask detection in white-box attacks.

Similarity measurement. Now we turn to the discussion upon the similarity measurement before and after adding adversarial textures. The value of similarity is calculated by comparing with images obtained by DM, so we only calculate similarity scores for AdvNoise-DM and MF^{2}M. We choose SSIM and PSNR as our similarity metrics, evaluating the similarity from aspects of visual error and structure difference. The SSIM of AdvNoise-DM and MF^{2}M are 0.9808 and 0.9812, respectively, indicating the high structural similarity in the reconstruction process. In terms of PSNR, the value of MF^{2}M is 40.45, higher than 38.76 of AdvNoise-DM, which is in line with the cognitive experience that the filtering operation has a more imperceptible modification to images.

Table 2: Multifaceted evaluation of each masking method on black-box attack. "Rank 1" refers to the top-1 identification rate and "Veri." refers to the TAR at 10^{-6} FAR.

	CosFace ResNet50			CosFace ResNet34		
	Face Rec.	Face Verification		Face Rec.	Face Verification	
	Rank 1	Veri.	AUC	Rank 1	Veri.	AUC
Solid-color	0.8207	0.8233	0.9991	0.7641	0.7697	0.9987
FGSM	0.7585	0.7624	0.9988	0.7147	0.7212	0.9984
I-FGSM	0.6720	0.6752	0.9978	0.6243	0.6303	0.9967
MI-FGSM	0.6419	0.6445	0.9972	0.6020	0.6077	0.9961
TI-FGSM	0.7640	0.7711	0.9988	0.7142	0.7214	0.9984
TI-MI-FGSM	0.6416	0.6438	0.9972	0.5996	0.6038	0.9958
DI^2-FGSM	0.7178	0.7222	0.9983	0.6699	0.6777	0.9977
M-DI^2-FGSM	0.6559	0.6592	0.9974	0.6165	0.6242	0.9963
DM (ours)	0.6400	0.6520	0.9971	0.5987	0.6126	0.9971
AdvNoise-DM (ours)	0.0726	0.0723	0.9293	0.0657	0.0622	0.9310
MF^{2}M (ours)	**0.0674**	**0.0670**	**0.9237**	**0.0546**	**0.0508**	**0.9212**

Table 3: Multifaceted evaluation of *physical* white-box attacks. "Rank 1" refers to the top-1 identification rate and "Veri." refers to the TAR at 10^{-6} FAR.

	Face Rec.	Face Verification		Mask Detection
	Rank 1	Veri.	AUC	Mask Rate
Solid-color (phys.)	0.7302	0.7398	0.9985	100%
DM (phys.)	0.5574	0.5550	0.9975	10%
I-FGSM (phys.)	0.2284	0.2497	0.9453	95%
AdvNoise-DM (phys.)	**0.0000**	**0.0000**	**0.6879**	**10%**
MF^{2}M (phys.)	**0.0000**	**0.0000**	**0.6658**	**10%**

Table 4: Multifaceted evaluation of *physical* black-box attacks. "Rank 1" refers to the top-1 identification rate and "Veri." refers to the TAR at 10^{-6} FAR.

	CosFace ResNet50			CosFace ResNet34		
	Face Rec.	Face Verification		Face Rec.	Face Verification	
	Rank 1	Veri.	AUC	Rank 1	Veri.	AUC
Solid-color (phys.)	0.7740	0.7846	0.9992	0.7586	0.7670	0.9993
DM (phys.)	0.7527	0.7369	0.9987	0.6757	0.6739	0.9985
I-FGSM (phys.)	0.6686	0.6791	0.9958	0.6734	0.6438	0.9951
AdvNoise-DM (phys.)	0.2189	0.2184	0.9683	0.1858	0.1860	0.9627
MF^{2}M (phys.)	**0.1692**	**0.1818**	**0.9670**	**0.1633**	**0.1336**	**0.9498**

4.3 Comparison on Black-box Attack Transferability

To verify the transferability of our methods, we utilize generated masked images to carry out black-box attacks. We conduct black-box attacks against face recognition models pre-trained under Cosface with ResNet34 and ResNet50 as the backbone. Curves with dots and without dots in Fig. 6 represent results of attacking ResNet34 and ResNet50, respectively. Compared with the "Rank 1" of AdvNoise-DM and MF^{2}M in Fig. 5(a) (nearly zero), they vary from 0.05 to 0.08 in Fig. 6(a). It shows that the interference degree to face recognizers in black-box attacks reduces, but is still strong, *i.e.*, our adversarial masking methods have sufficient transferability. Besides, curves of MF^{2}M are lower than curves of AdvNoise-DM targeting the same model, indicating MF^{2}M has stronger transferability. Compared with adversarial attack baselines, AdvNoise-DM and MF^{2}M have absolute advantages in the impact on face recognizers as shown in Table 2.

4.4 Extension to Physical Attack

Due to various COVID-19 related restrictions, we were not able to recruit human subjects to study the effect of physical attack by wearing our proposed faced masks. Therefore, we use an alternative recapture method to illustrate the physical effects of our proposed masking methods. We randomly select 20 faces of different identities from the FaceScrub dataset as origin images in Fig. 7(a). We process the 20 faces with our proposed MF^{2}M and obtain digital attacked faces as shown in Fig. 7(b). Then we use an *ApeosPort − IVC*5575 printer to print these attacked images and recapture images like Fig. 7(c), which has obvious color differences from Fig. 7(b). This procedure is meant for methodologically mimicking the process of plastering the patterns from a digital medium onto a physical one, such as fabric, linen, or paper, so that the physical appearance can be digitally reacquired via image sensors. Finally, we resize the recaptured images to the size of 112×112, extract faced masks from them, overlay faced masks to the 20 corresponding original faces, and obtain images used in the physical attack as shown in Fig. 7(d). Based on this synthesis process, we conduct the experiment of physical attacks and demonstrate the robustness of our proposed MF^{2}M and AdvNoise-DM to evade face recognition and mask detection. Except for the solid-color medical mask and DM, we choose *I-FGSM baseline* (*i.e.*, apply I-FGSM to solid-color masks), which is the strongest baseline in digital attacks, as the main baseline for the

physical attacks. We also process these masking methods by the method shown in Fig. 7 and set three baselines in physical attacks.

For the physical white-box attack, the second column and the third column of Table 3 show that the top-1 identification rates and the TAR at 10^{-6} FAR of MF^{2}M and AdvNoise-DM are both zero, indicating the strong interference of these two masking methods to the face recognizer. The last column of Table 3 shows that only 10% of images by MF^{2}M and AdvNoise-DM are detected faced masks, demonstrating the powerful ability of our proposed masking methods in avoiding mask detection in physical white-box attack. The corresponding CMC curves in Fig. 8(a) illustrate that the identification rates of MF^{2}M and AdvNoise-DM are always below three baselines at different ranks. The ROC curves in Fig. 8(b) show that the TPR of MF^{2}M and AdvNoise-DM are always less than three baselines at different FPR.

As for the physical black-box attack, the top-1 identification rates and the TAR at 10^{-6} FAR of *I-FGSM baseline* are more than 0.64 as shown in Table 4. It indicates that the adversarial textures added in *I-FGSM baseline* almost failed. In contrast, these metrics of our proposed MF^{2}M and AdvNoise-DM are still less than 0.22, indicating our proposed masking methods remain highly interference to face recognizers in physical black-box attack. Compared with AdvNoise-DM, MF^{2}M has a greater influence on face recognizers. The corresponding CMC curves and ROC curves of physical black-box attack are shown in Fig. 9.

4.5 Ablation Study and Discussion

In AdvNoise-DM, we only do noise-based adversarial attacks, and the intensity of noise reaches 0.04. When we combine noise-based and filtering-based attacks in MF^{2}M, we only need lower noise intensity (*i.e.*, 0.01) to achieve similar results in face recognition. We experiment under different attack intensities and compare these two methods in the PSNR-AUC curves. As shown in Fig. 10(a), MF^{2}M (orange curve) gets higher PSNR values than AdvNoise-DM (blue curve) at the same AUC values, indicating the advantage of MF^{2}M in naturalness. We also conduct experiments on attacking
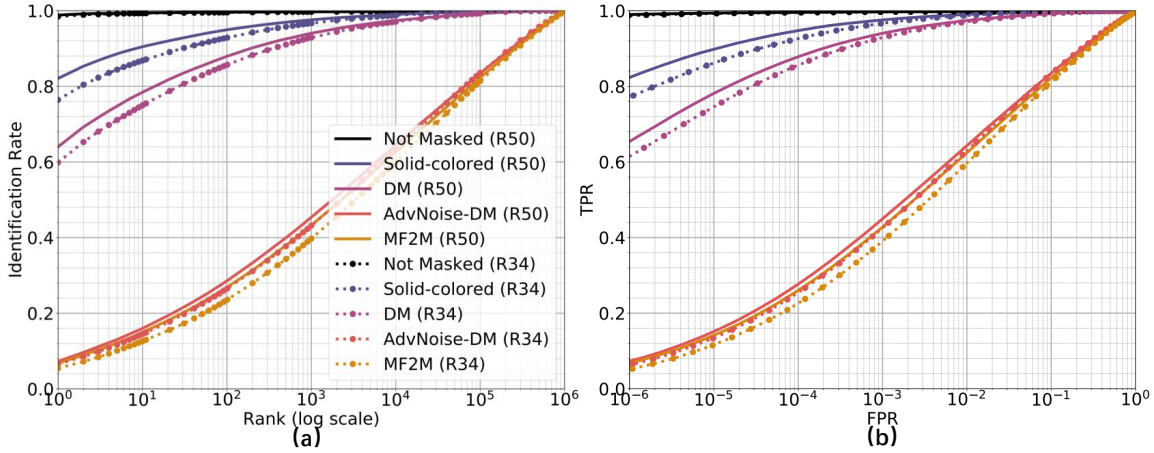
Figure 6: The effects of different masking methods on face recognition in black-box attacks. (a) The CMC curves of the face identification task. (b) The ROC curves of the face verification task. The abscissa and ordinate are consistent with Fig. 5. R34 and R50 in the legend indicate that ResNet34 and ResNet50 are separately used as the backbone.
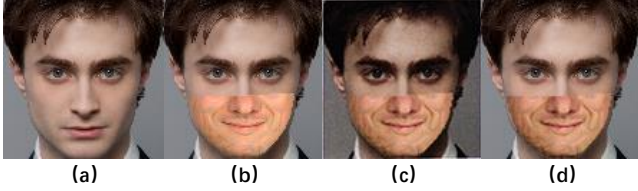

Figure 7: The process of synthesizing the image in the physical attack. (a) The original image in the FaceScrub dataset. (b) The digital image by MF^2M. (c) The recaptured image. (d) Extract the faced mask from (c) and overlay it to (a), used in the physical attack.

Figure 9: The effects of different masking methods on face recognition in *physical* black-box attacks. (a) The CMC curves of the face identification task. (b) The ROC curves of the face verification task. The abscissa and ordinate are consistent with Fig. 5. R34 and R50 in the legend indicate that ResNet34 and ResNet50 are separately used as the backbone.
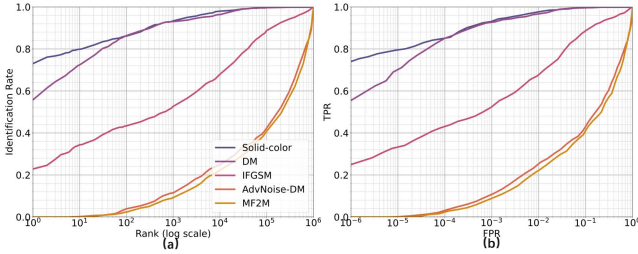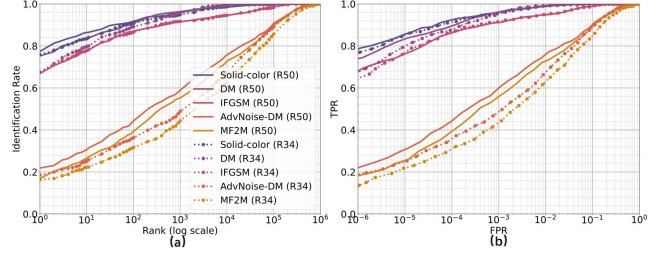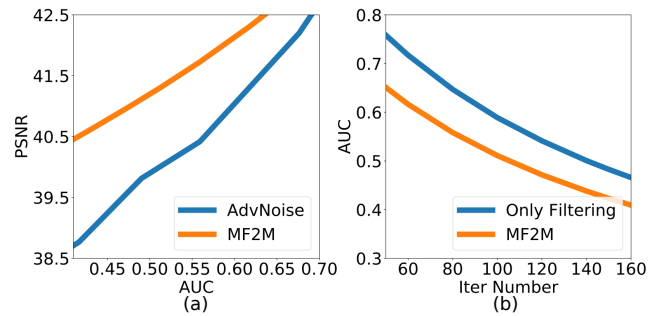

Figure 8: The effects of different masking methods on face recognition in *physical* white-box attacks. (a) The CMC curves of the face identification task. (b) The ROC curves of the face verification task. The abscissa and ordinate are consistent with Fig. 5.

Figure 10: (a) PSNR at different AUC of AdvNoise-DM and MF^2M. (b) AUC at different iteration numbers of MF^2M and the method only using filtering kernels.

images by only utilizing filtering kernels and show the comparison in Fig. 10(b). At the same number of iterations for altering kernels, MF^2M (orange curve) achieves lower AUC values than the method only using filtering kernels (blue curve). This shows that adding noise can assist the optimization of filtering kernels as noise-based attacks have fewer parameters and higher attack efficiency.

5 CONCLUSIONS

In this paper, we propose MF^2M, an adversarial masking framework that adds faced masks containing partial face patterns and special adversarial textures. Our work reveals the potential risks of existing face recognizers and mask detectors regarding facial masks specially customized. The reconstructed images from our methods retain enough naturalness, generating a higher safety hazard. Therefore, particularly generated facial masks should be taken into consideration when designing the FRS and mask detection systems.

REFERENCES

[1] Borut Batagelj, Peter Peer, Vitomir Štruc, and Simon Dobrišek. 2021. How to Correctly Detect Face-Masks for COVID-19 from Visual Information? *Applied Sciences* 11, 5 (2021), 2070.

[2] Fadi Boutros, Naser Damer, Florian Kirchbuchner, and Arjan Kuijper. 2021. Unmasking Face Embeddings by Self-restrained Triplet Loss for Accurate Masked Face Recognition. *arXiv preprint arXiv:2103.01716* (2021).

[3] Fadi Boutros, Naser Damer, Jan Niklas Kolf, Kiran Raja, Florian Kirchbuchner, Raghavendra Ramachandra, Arjan Kuijper, Pengcheng Fang, Chao Zhang, Fei Wang, et al. 2021. MFR 2021: Masked Face Recognition Competition. In *2021 IEEE International Joint Conference on Biometrics (IJCB)*. IEEE, 1–10.

[4] Qiong Cao, Li Shen, Weidi Xie, Omkar M Parkhi, and Andrew Zisserman. 2018. Vggface2: A dataset for recognising faces across pose and age. In *2018 13th IEEE international conference on automatic face & gesture recognition (FG 2018)*. IEEE, 67–74.

[5] Jiankang Deng, Jia Guo, Xue Niannan, and Stefanos Zafeiriou. 2019. ArcFace: Additive Angular Margin Loss for Deep Face Recognition. In *CVPR*.

[6] Jiankang Deng, Jia Guo, Niannan Xue, and Stefanos Zafeiriou. 2021. Pytorch implementation of Face Recognition Model under ArcFace. https://github.com/deepinsight/insightface/tree/master/recognition/arcface_torch.

[7] Jiankang Deng, Jia Guo, Niannan Xue, and Stefanos Zafeiriou. 2021. Pytorch Implementation of predicting 2d-106 landmark coordinates. https://github.com/deepinsight/insightface/tree/master/alignment/coordinate_reg.

[8] dominhhieu1019. 2021. Pytorch implementation of Face Recognition Model under CosFace. https://github.com/dominhhieu1019/arcface_torch.

[9] Yinpeng Dong, Fangzhou Liao, Tianyu Pang, Hang Su, Jun Zhu, Xiaolin Hu, and Jianguo Li. 2018. Boosting adversarial attacks with momentum. In *CVPR*. 9185–9193.

[10] Yinpeng Dong, Tianyu Pang, Hang Su, and Jun Zhu. 2019. Evading defenses to transferable adversarial examples by translation-invariant attacks. In *CVPR*. 4312–4321.

[11] Ruijun Gao, Qing Guo, Qian Zhang, Felix Juefei-Xu, Hongkai Yu, and Wei Feng. 2021. Adversarial Relighting against Face Recognition. *arXiv preprint arXiv:2108.07920* (2021).

[12] Shiming Ge, Jia Li, Qiting Ye, and Zhao Luo. 2017. Detecting masked faces in the wild with lle-cnns. In *Proceedings of the IEEE conference on computer vision and pattern recognition*. 2682–2690.

[13] Ian J Goodfellow, Jonathon Shlens, and Christian Szegedy. 2014. Explaining and harnessing adversarial examples. *arXiv preprint arXiv:1412.6572* (2014).

[14] Qing Guo, Ziyi Cheng, Felix Juefei-Xu, Lei Ma, Xiaofei Xie, Yang Liu, and Jianjun Zhao. 2021. Learning to Adversarially Blur Visual Object Tracking. In *ICCV*. 10839–10848.

[15] Qing Guo, Felix Juefei-Xu, Xiaofei Xie, Lei Ma, Jian Wang, Bing Yu, Wei Feng, and Yang Liu. 2020. Watch out! Motion is Blurring the Vision of Your Deep Neural Networks. In *Advances in Neural Information Processing Systems (NeurIPS)*.

[16] Felix Juefei-Xu. 2018. Unconstrained Periocular Face Recognition: From Reconstructive Dictionary Learning to Generative Deep Learning and Beyond. *PhD Dissertation, Carnegie Mellon University* (2018).

[17] Felix Juefei-Xu, Khoa Luu, and Marios Savvides. 2015. Spartans: Single-sample periocular-based alignment-robust recognition technique applied to non-frontal scenarios. *IEEE Transactions on Image Processing* 24, 12 (2015), 4780–4795.

[18] Felix Juefei-Xu, Dipan K Pal, and Marios Savvides. 2014. Hallucinating the full face from the periocular region via dimensionally weighted K-SVD. In *Proceedings of the IEEE Conference on Computer Vision and Pattern Recognition Workshops*. 1–8.

[19] Felix Juefei-Xu and Marios Savvides. 2014. Subspace-based discrete transform encoded local binary patterns representations for robust periocular matching on NIST's face recognition grand challenge. *IEEE transactions on image processing* 23, 8 (2014), 3490–3505.

[20] Felix Juefei-Xu and Marios Savvides. 2016. Fastfood dictionary learning for periocular-based full face hallucination. In *2016 IEEE 8th International Conference on Biometrics Theory, Applications and Systems (BTAS)*. IEEE, 1–8.

[21] Tero Karras, Samuli Laine, and Timo Aila. 2019. A style-based generator architecture for generative adversarial networks. In *Proceedings of the IEEE Conference on Computer Vision and Pattern Recognition*. 4401–4410.

[22] Ira Kemelmacher-Shlizerman, Steven M Seitz, Daniel Miller, and Evan Brossard. 2016. The megaface benchmark: 1 million faces for recognition at scale. In *Proceedings of the IEEE conference on computer vision and pattern recognition*. 4873–4882.

[23] Stepan Komkov and Aleksandr Petiushko. 2021. Advhat: Real-world adversarial attack on arcface face id system. In *2020 25th International Conference on Pattern Recognition (ICPR)*. IEEE, 819–826.

[24] Alexey Kurakin, Ian Goodfellow, and Samy Bengio. 2016. Adversarial machine learning at scale. *arXiv preprint arXiv:1611.01236* (2016).

[25] Yande Li, Kun Guo, Yonggang Lu, and Li Liu. 2021. Cropping and attention based approach for masked face recognition. *Applied Intelligence* 51, 5 (2021), 3012–3025.

[26] Tsung-Yi Lin, Priya Goyal, Ross Girshick, Kaiming He, and Piotr Dollár. 2017. Focal loss for dense object detection. In *Proceedings of the IEEE international conference on computer vision*. 2980–2988.

[27] Weiyang Liu, Yandong Wen, Zhiding Yu, Ming Li, Bhiksha Raj, and Le Song. 2017. Sphereface: Deep hypersphere embedding for face recognition. In *Proceedings of the IEEE conference on computer vision and pattern recognition*. 212–220.

[28] Weiyang Liu, Yandong Wen, Zhiding Yu, and Meng Yang. 2016. Large-margin softmax loss for convolutional neural networks.. In *ICML*, Vol. 2. 7.

[29] Mohamed Loey, Gunasekaran Manogaran, Mohamed Hamed N Taha, and Nour Eldeen M Khalifa. 2021. A hybrid deep transfer learning model with machine learning methods for face mask detection in the era of the COVID-19 pandemic. *Measurement* 167 (2021), 108288.

[30] Aleksander Madry, Aleksandar Makelov, Ludwig Schmidt, Dimitris Tsipras, and Adrian Vladu. 2017. Towards deep learning models resistant to adversarial attacks. *arXiv preprint arXiv:1706.06083* (2017).

[31] Satya Mallick. 2015. Delaunay Triangulation and Voronoi Diagram using OpenCV (C++ / Python). https://learnopencv.com/delaunay-triangulation-and-voronoi-diagram-using-opencv-c-python.

[32] David Montero, Marcos Nieto, Peter Leskovsky, and Naiara Aginako. 2021. Boosting Masked Face Recognition with Multi-Task ArcFace. *arXiv preprint arXiv:2104.09874* (2021).

[33] Mei Ngan, Patrick Grother, and Kayee Hanaoka. 2020. Ongoing Face Recognition Vendor Test (FRVT) Part 6B: Face recognition accuracy with face masks using post-COVID-19 algorithms. https://doi.org/10.6028/NIST.IR.8331

[34] Omkar M. Parkhi, Andrea Vedaldi, and Andrew Zisserman. 2015. Deep Face Recognition. In *Proceedings of the British Machine Vision Conference (BMVC)*. BMVA Press, Article 41, 12 pages.

[35] Bosheng Qin and Dongxiao Li. 2020. Identifying facemask-wearing condition using image super-resolution with classification network to prevent COVID-19. *Sensors* 20, 18 (2020), 5236.

[36] Mahmood Sharif, Sruti Bhagavatula, Lujo Bauer, and Michael K Reiter. 2016. Accessorize to a crime: Real and stealthy attacks on state-of-the-art face recognition. In *Proceedings of the 2016 acm sigsac conference on computer and communications security*. 1528–1540.

[37] simpletask1. 2020. Pytorch Implementation of Retinanet for Face Mask Detection. https://github.com/simpletask1/Retinanet-face_mask_detection.

[38] Yi Sun, Xiaogang Wang, and Xiaoou Tang. 2014. Deep learning face representation from predicting 10,000 classes. In *Proceedings of the IEEE conference on computer vision and pattern recognition*. 1891–1898.

[39] Yaniv Taigman, Ming Yang, Marc'Aurelio Ranzato, and Lior Wolf. 2014. Deepface: Closing the gap to human-level performance in face verification. In *Proceedings of the IEEE conference on computer vision and pattern recognition*. 1701–1708.

[40] Binyu Tian, Felix Juefei-Xu, Qing Guo, Xiaofei Xie, Xiaohong Li, and Yang Liu. 2021. AVA: Adversarial Vignetting Attack against Visual Recognition. *arXiv preprint arXiv:2105.05558* (2021).

[41] Feng Wang, Jian Cheng, Weiyang Liu, and Haijun Liu. 2018. Additive margin softmax for face verification. *IEEE Signal Processing Letters* 25, 7 (2018), 926–930.

[42] Hao Wang, Yitong Wang, Zheng Zhou, Xing Ji, Dihong Gong, Jingchao Zhou, Zhifeng Li, and Wei Liu. 2018. Cosface: Large margin cosine loss for deep face recognition. In *Proceedings of the IEEE conference on computer vision and pattern recognition*. 5265–5274.

[43] Run Wang, Felix Juefei-Xu, Qing Guo, Yihao Huang, Xiaofei Xie, Lei Ma, and Yang Liu. 2020. Amora: Black-box adversarial morphing attack. In *ACM-MM*. 1376–1385.

[44] Zhou Wang, Alan C Bovik, Hamid R Sheikh, and Eero P Simoncelli. 2004. Image quality assessment: from error visibility to structural similarity. *IEEE transactions on image processing* 13, 4 (2004), 600–612.

[45] Zhanxiong Wang, Keke He, Yanwei Fu, Rui Feng, Yu-Gang Jiang, and Xiangyang Xue. 2017. Multi-task deep neural network for joint face recognition and facial attribute prediction. In *Proceedings of the 2017 ACM on International Conference on Multimedia Retrieval*. 365–374.

[46] Zhongyuan Wang, Guangcheng Wang, Baojin Huang, Zhangyang Xiong, Qi Hong, Hao Wu, Peng Yi, Kui Jiang, Nanxi Wang, Yingjiao Pei, et al. 2020. Masked face recognition dataset and application. *arXiv preprint arXiv:2003.09093* (2020).

[47] Yandong Wen, Kaipeng Zhang, Zhifeng Li, and Yu Qiao. 2016. A discriminative feature learning approach for deep face recognition. In *European conference on computer vision*. Springer, 499–515.

[48] Cihang Xie, Zhishuai Zhang, Yuyin Zhou, Song Bai, Jianyu Wang, Zhou Ren, and Alan L Yuille. 2019. Improving transferability of adversarial examples with input diversity. In *Proceedings of the IEEE/CVF Conference on Computer Vision and Pattern Recognition*. 2730–2739.

[49] Bangjie Yin, Wenxuan Wang, Taiping Yao, Junfeng Guo, Zelun Kong, Shouhong Ding, Jilin Li, and Cong Liu. 2021. Adv-Makeup: A New Imperceptible and Transferable Attack on Face Recognition. *arXiv preprint arXiv:2105.03162* (2021).

[50] Xiao Zhang, Zhiyuan Fang, Yandong Wen, Zhifeng Li, and Yu Qiao. 2017. Range loss for deep face recognition with long-tailed training data. In *Proceedings of the IEEE International Conference on Computer Vision*. 5409–5418.